NJC

Accepted Manuscript

This is an *Accepted Manuscript*, which has been through the Royal Society of Chemistry peer review process and has been accepted for publication.

Accepted Manuscripts are published online shortly after acceptance, before technical editing, formatting and proof reading. Using this free service, authors can make their results available to the community, in citable form, before we publish the edited article. We will replace this *Accepted Manuscript* with the edited and formatted *Advance Article* as soon as it is available.

You can find more information about *Accepted Manuscripts* in the Information for Authors.

Please note that technical editing may introduce minor changes to the text and/or graphics, which may alter content. The journal's standard Terms & Conditions and the Ethical guidelines still apply. In no event shall the Royal Society of Chemistry be held responsible for any errors or omissions in this *Accepted Manuscript* or any consequences arising from the use of any information it contains.

ROYAL SOCIETY OF CHEMISTRY

www.rsc.org/njc

Effective solar-based iron oxide supported HY zeolite catalyst for decolorization of organic and simulated dyes

Norzahir Sapawe

Section of Technical Foundation, Universiti Kuala Lumpur – Malaysian Institute of Chemical and Bioengineering Technology, Lot 1988 Vendor City, Taboh Naning, 78000 Alor Gajah, Melaka, MALAYSIA.

*To whom correspondence should be addressed,

Norzahir Sapawe (Ph.D.)

Tel : +6013-575-7795 Fax: +606-551-2001

Email : norzahir@unikl.edu.my ; za_heer86@yahoo.com

Abstract

Highly dispersed of electrogenerated nanoparticles iron oxide onto HY zeolite ($EGFe_2O_3$/HY) was prepared by a facile electrochemical method, and has been characterized using XRD, TEM, BET, and UV–vis/DRS. The formation of $EGFe_2O_3$ nanoparticles <30 nm in size and well distributed on the surface of HY, led to enhanced the catalytic activity for decolorization of organic dyes such as methylene blue (MB), Congo red (CR), and methyl orange (MO) under sunlight irradiation. The MB dye shows the highest decolorization (99.9%) followed by CR (96.4%) and MO (91.3%). Kinetics study signifies that the reaction follows pseudo first–order kinetics, and the rate constants was determined using the Langmuir–Hinshelwood model that gave K_R = 0.48 mg $L^{-1}h^{-1}$, K_{LH} = 3.83 L mg^{-1} for MB; K_R = 0.39 mg $L^{-1}h^{-1}$, K_{LH} = 1.78 L mg^{-1} for CR; and K_R = 0.29 mg $L^{-1}h^{-1}$, K_{LH} = 0.13 L mg^{-1} for MO. There is no dissolution of $EGFe_2O_3$ ions was detected during the photoreaction. The catalyst was stable with a slightly decrease of decolorization (<13%) after five cycling runs. Good performance of decolorization of simulated dyes was observed with nearly complete mineralization as measured by COD and TOC removal.

***Keywords*:** nanoparticles; $EGFe_2O_3$; electrochemical; photodecolorization; organic dyes

1. Introduction

Large amount of dyes were synthesized in this recent time to be used for many industries such as textiles, papers, cosmetics, plastics, and etc. More than 10, 000 dyes with a total per annum productions over 7×10^5 MT worldwide are commercially available with nearly 15% of dyestuffs are released in textile effluents [1,2]. The discharge of these highly coloured substances hindered the light penetration in the stream, subsequently disturbed the biological processes and also aquatic life. Numerous approaches have been developed for the removal of these pollutants from water bodies, such as the conventional biological and physical treatment [3-8]. However, these methods were unproductive and have their own limitations including led to the generation of secondary pollutants.

The use of semiconductor metal oxides such as TiO_2, ZnO, Fe_2O_3, ZrO_2, etc. under advanced oxidation processes (AOPs) have been employed, and become popular in recent years because they can convert various types of dye compounds into non–toxic products, CO_2 and water at ambient temperatures [2,9-12]. The generation of OH radicals plays an important role in the photoreaction which led to complete degradation and mineralization [13]. Utilization of Fe_2O_3 as tremendous photocatalyst have been widely studied due to its unique properties such as nanosized in range, high surface area, superparamagnetism, low toxicity, chemically inertness, and biocompatibility [14-16].

The mesoporous materials such as zeolite have become the focus of intensive research as a support for metal oxides (TiO_2–HZSM5, Co–ZSM5 and CuO–X) because they influence the catalytic performance through structural features [17-19]. These zeolitic materials offer high surface areas, thermally stable, eco–friendly in nature, and also have specific photophysical properties for controlling charge– and electron–transfer processes [20,21]. In addition to

lessening the amount of metal oxide required, the relationship between zeolite and metal oxides also leads to the enhancement of the contact between the catalyst surface and irradiation [9].

We have reported on the preparation method for electrogenerated metal oxides supported HY catalyst by a simple and rapid electrochemical process, which possesses high photoactivity in the decolorization of dyes [22-25]. The nanosized metal oxides were found to play important roles in the enhancement of the reaction [22,25]. Therefore, herein, we report the facile synthesis of highly dispersed electrogenerated nanoparticles of a Fe_2O_3 onto HY ($EGFe_2O_3$/HY) catalyst, and its remarkable performance toward the photodecolorization of various types of organic dye, such as methylene blue (MB), congo red (CR), and methyl orange (MO). The 1 wt% $EGFe_2O_3$/HY catalyst was electrosynthesized within a short time that less than 2 min. The catalyst was characterized by X–ray diffraction (XRD), transmission electron microscopy (TEM), Brunnauer–Emmett–Teller surface area (BET), and ultraviolet–visible diffuse reflectance spectroscopy (UV–vis/DRS). The photoactivity of the catalyst for decolorization of MB, CR, and MO was studied under various conditions to determine the effect of pH, catalyst dosage, and initial dye concentrations. The kinetics study, dissolution of iron (leaching), regeneration, and biodegradability of the system as well as an appropriate proposed photocatalytic mechanism were discussed in details. The photocatalytic decolorization validation of catalyst performance and application of the system under the simulated dyes was also investigated.

2. Experimental

2.1. Materials

The HY zeolite had a Si/Al ratio of 80 and was purchased from Zeolyst International. *N,N*–dimethylformamide (DMF) was purchased from Merck and naphthalene was obtained from Fluka. Sodium hydroxide (NaOH), hydrochloric acid (HCl), methylene blue (MB), congo red (CR), and methyl orange (MO) were obtained from QReC^{TM}. The platinum (Pt) and iron (Fe) plate cells were obtained from Nilaco Metal, Japan (>99% purity). All reagents were of analytical grade and were used as received. Deionized water was used for the preparation of the pH solution and adjustments to the pH were performed using 0.1M HCl and NaOH solutions.

2.2. Catalyst preparation

1 wt% EGFe_2O_3/HY catalyst was prepared according to the previous reported procedure [12,22-25]. A 10 mL of DMF solution containing 0.1 M tetraethylammonium perchlorate was electrolyzed in the presence of 6 mmol naphthalene as a mediator and 1.5 g HY zeolite in a normal one–compartment cell fitted with a Pt plate cathode (2 × 2 cm^2) and a Fe plate anode (2 × 2 cm^2) at a constant current density of 120 mA/cm^2 under a nitrogen atmosphere at 273 K. Naphthalene was used as a mediator in the system to produce radical anions, which then reduced the iron cations from the anode to give iron nanoparticles (Fe^0). After electrolysis the mixture was impregnated, oven dried overnight at 378 K, and calcined at 823 K for 3 h to yield a white powder, EGFe_2O_3/HY catalyst, which ready for characterization and photocatalytic testing.

The bare EGFe_2O_3 were prepared using the same procedure as above but in the absence of HY zeolite. The required weight percent of the EGFe_2O_3 supported on HY was calculated by the time of electrolysis, which is based on the Faraday's law,

$$t = \left(\frac{F}{I}\right)(z \times n) \quad (1)$$

where t = total time for the constant current applied (s); F = 96486 C mol^{-1}, which is the Faraday constant; I = the electric current applied (mA); z = the valency number of ions of iron (electrons transferred per ion); and n = the number of moles of iron (number of moles, liberated n = m/M).

2.3. Characterization

The crystalline structures of the catalysts were studied by XRD recorded on a D8 ADVANCE Bruker X–ray diffractometer using Cu K_α radiation at a 2θ angle ranging from 3° to 90°. The particle sizes of the catalyst were calculated using the Debye–Scherrer equation:

$$D = \frac{k\lambda}{\beta \cos\theta} \quad (2)$$

where k = 0.94 is a coefficient, λ = 1.5406 Å is the X-ray wavelength, β is the full width half maximum (FWHM) of the sample and θ is the diffracting angle. The phases were identified with the aid of the Joint Committee on Powder Diffraction Standards (JCPDS) files.

The morphological properties of the EGFe_2O_3/HY catalyst were examined by TEM (JEOL JEM–2100F). The textural properties were determined from nitrogen adsorption–desorption isotherms at the temperature of liquid nitrogen using a Micromeritics ASAP 2010 instrument. The nitrogen adsorption–desorption isotherm and Barrett–Joyner–Halender (BJH) pore distributions were calculated from the desorption branch of the nitrogen isotherm of the samples. Prior to measurement, all the samples were degassed at 383 K to 0.1Pa. The optical absorption properties of the catalyst were obtained using a UV–vis DRS (Perkin Elmer Spectrophotometer)

in the range of 200–800 nm at room temperature. The band gap of $EGFe_2O_3$ was determined from plots of the Kubelka–Munk (K–M) function [$f_{K\text{-}M} = (h\nu/\lambda)^{1/2}$] as a function of the energy of the excitation light [hν].

2.4. Photocatalytic testing

The photocatalytic activity of the prepared $EGFe_2O_3$/HY catalyst was tested for the decolorization of MB, CR, and MO. A 0.08 g sample of the $EGFe_2O_3$/HY was dispersed in 200 mL of 10 mg L^{-1} dye aqueous solutions. The adsorption–desorption equilibrium was achieved under dark conditions after 1 h, and the mixture was then exposed for 2 h with constant stirring under sunlight (January to March 2013, between 12 NN until 3 PM). The average intensity of sunlight during this period is 1.315 x 10^5 Lux unit. Irradiation was carried out in the open air conditions. However, during the illumination time, no volatility of the solvent was observed.

At specific time intervals, 2.5 mL of the sample solution was withdrawn and centrifuged prior to measurements of the dye concentration using a UV–vis spectrophotometer (Agilent Technologies Cary 60 UV–vis) using the characteristic adsorption band at 664 nm, 496 nm, and 464 nm; for MB, CR, and MO, respectively. The decolorization percentage was calculated as follows:

$$Decolorization\ (\%) = \frac{(C_0 - C_t)}{C_0} \times 100 \quad (3)$$

where C_o represents the initial concentration and C_t denotes a variable concentration.

2.5. Analyses

The elemental analyses of Fe in a solution during an experiment were determined by ICP–MS using ELAN 6100 Perkin Elmer ICPMS. The HACH DR4000 spectrometer was used for COD measurement, whereas the total organic carbon (TOC) removal was determined using a TOC Shimadzu Vcph spectrophotometer for each run before and after a 1 h reaction time for the evaluation of the mineralization of dyes. TOC was calculated as the difference between the total carbon (TC) and inorganic (IC) in the liquid sample.

3. Results and Discussion

In this study, single metal oxide, iron nanoparticles supported HY zeolite catalyst was synthesized using a simple electrochemical method, and denoted as EGFe_2O_3/HY. The characterizations of the catalysts were done by XRD, TEM, EDX, BET, UV-vis DRS, and XPS. The activity of the catalysts for the photodecolorization of methylene blue (MB), congo red (CR), and methyl orang (MO) were studied under various conditions to determine the effect of pH, catalyst dosage, and initial dye concentration, and were exposed under sunlight irradiation. The kinetics modelling of the photodecolorization was described, and the stability of catalysts was conducted in term of reusability and leaching effect. Then, the mineralization of simulated dyes (MB, CR, and MO) were measured with TOC and COD analyses. Finally, the reaction mechanism of photocatalytic activity was proposed.

3.1. Characterization

3.1.1 Crystallinity, phase, and structural studies

The XRD pattern of the prepared $EGFe_2O_3$/HY catalyst was compared with bare HY, and the results are shown in Fig. 1a. The peak intensity of HY decreased as the $EGFe_2O_3$ were loaded onto HY, suggesting that the presence of foreign substances affected the morphology of the supported HY fingerprint. No obvious diffraction peaks of $EGFe_2O_3$ could be identified in all ranges of XRD patterns, suggested that there are highly dispersed of nanoparticles or even amorphous $EGFe_2O_3$ species over the HY samples [26]. A series of peaks were observed at 24.2º (012), 33.1º (104), 35.6º (110), 40.8º (113), 49.5º (024), 54.1º (116), 62.6º (214), and 64.1º (300) which are consistent to the hematite phase of α−Fe_2O_3 with rhombohedral symmetry (JCPDS 33–0664) (Fig. 1b). There is no other diffraction peaks being detected, indicating the purity of the prepared catalyst [12,27]. The average crystallite size of the $EGFe_2O_3$ was estimated by the Debye–Scherrer equation on the basis of the major peaks at 33.1º (104) which were 26.5 nm.

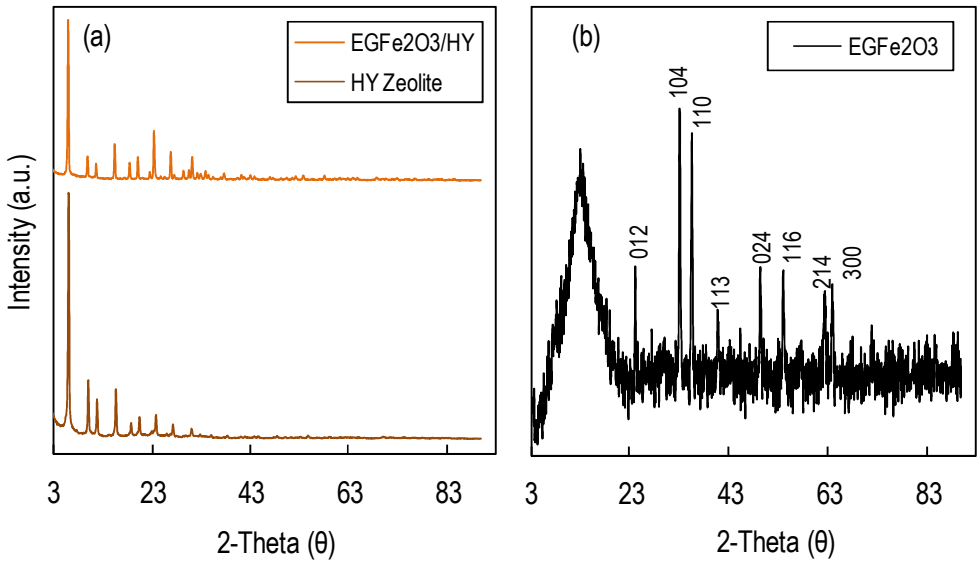

Fig. 1. XRD patterns of the (a) $EGFe_2O_3$/HY and (b) $EGFe_2O_3$ catalyst for full range 3–93º.

3.1.2 Morphological properties

The morphological properties of the $EGFe_2O_3$/HY catalyst was examined by TEM, and compared with pure HY zeolite, as shown in Fig. 2. The average particle size was observed for the $EGFe_2O_3$ which is varied in a narrow range from 5–30 nm, and the images are presented in Fig. 2a. The theoretical values of the particle sizes (D) were also found to be 15.2 nm, which were estimated by the following equation:

$$D = \frac{6}{\rho S} \quad (4)$$

where ρ is the theoretical density of the electrogenerated metal oxide powder and S is the surface area determined by N_2 adsorption–desorption isotherms, assuming that the particles are spherical in shape [28].

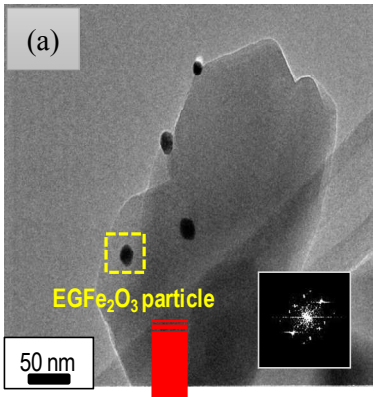

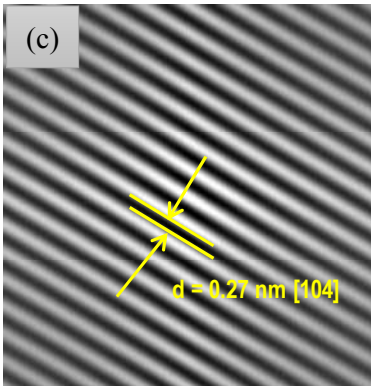

(b)

Element	Mass (%)
C	2.1
O	2.5
Pt	5.1
Fe	90.3
Total	100.0

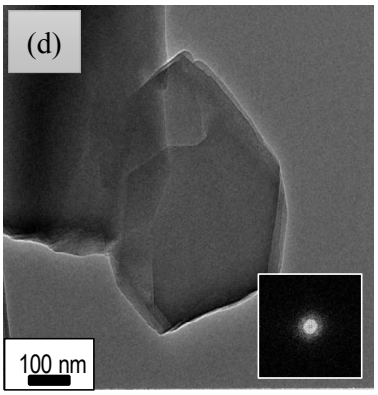

Fig. 2. HR–TEM micrographs of the (a, c) $EGFe_2O_3$/HY photocatalyst, (b) EDX analysis of elemental composition of $EGFe_2O_3$, and (d) HY zeolite in low and high magnification, and the insert figure is its corresponding FFT.

The inset image shows the fast Fourier transform patterns (FFT), and magnification of the selected area in the FFT patterns showed the atomic arrangement in the crystal, and allowed the estimation of the interplanar distances (Fig. 2c). The inter–planar distance value (*d*–spacing) of the lattice fringes estimated (0.27 nm) from this image was consistent with the value of lattice spacing of $EGFe_2O_3$, which was obtained from the XRD database software. This agreement confirms that the $EGFe_2O_3$ nanoparticles were deposited and well dispersed on the HY support as seen in Fig. 2a. In addition, the EDX analysis was employed to determine the composition of the $EGFe_2O_3$, and result was tabulated in inset table in Fig. 2b. The presence of Pt and C were corresponded to the coated material as well as the platform of the holder sample. No other element was detected indicating that the prepared $EGFe_2O_3$ is free from other impurities.

3.1.3 Study of optical properties

The optical properties of the respective catalysts were studied by UV–vis diffuse reflectance spectroscopy (UV–vis/DRS). $EGFe_2O_3$ catalyst shows a characteristic peak at 634 nm (Fig. 3a) which exhibited a red shift region, signifying that the photoreaction was suitable to be conducted under visible light region. The band gap energy of $EGFe_2O_3$ was also determined using the Kubelka–Munk (K–M) spectrum by plotting $f_{K-M} = (hc/\lambda)^2$ as a function of hν, and the results are shown in Fig. 3b [29]. The band gap value of the prepared $EGFe_2O_3$ catalysts was similar and agreed with those reported in the literatures [30].

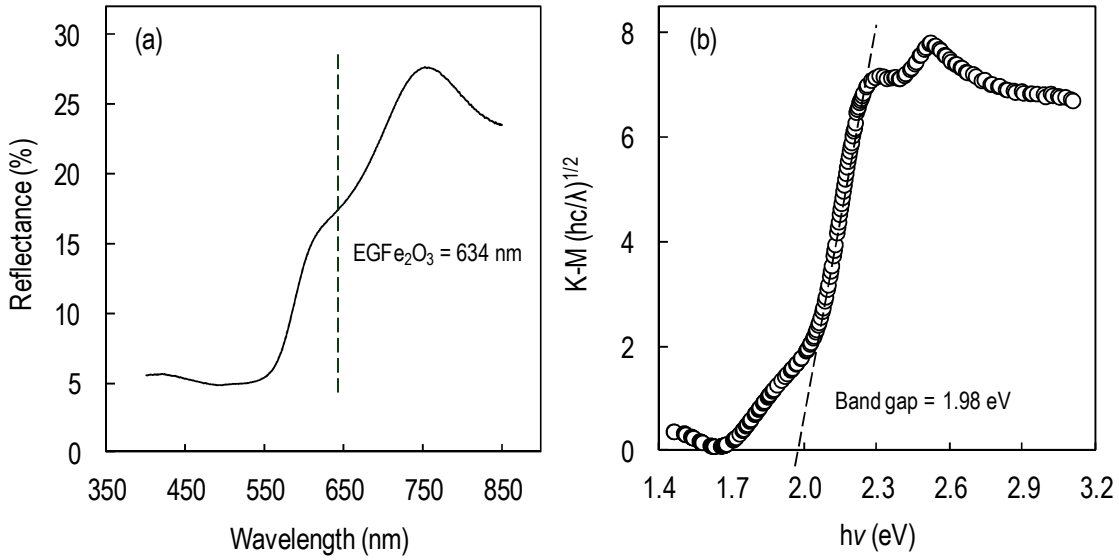

Fig. 3. (a) UV–vis reflectance and (b) the (f_{K-M}) vs. (hv) spectra of $EGFe_2O_3$ photocatalyst.

3.1.4 Study of textural properties

The surface area analysis (S.A.) data obtained from the BET method, as well as the pore volume (P.V.) and pore diameter (P.D.) determined by the Barret–Joyner–Halenda (BJH) desorption isotherms method are tabulated in insert table in Fig. 4. The addition of $EGFe_2O_3$ onto HY decreased the surface area, pore volume, and pore diameter. The decrease in pore volume was confirmed by the pore blockage as shown in Fig. 4 and maybe also due to a reflection of the uneven particle sizes of the catalyst. A smaller pore diameter was reported to enhance the photocatalytic activity [31]. Apart from that, a highly dispersed of $EGFe_2O_3$ onto HY confirmed by TEM analysis could be subsequently improved the surface contact of the catalyst and enhanced the light irradiation, thereby increased the photodecolorization of the dyes.

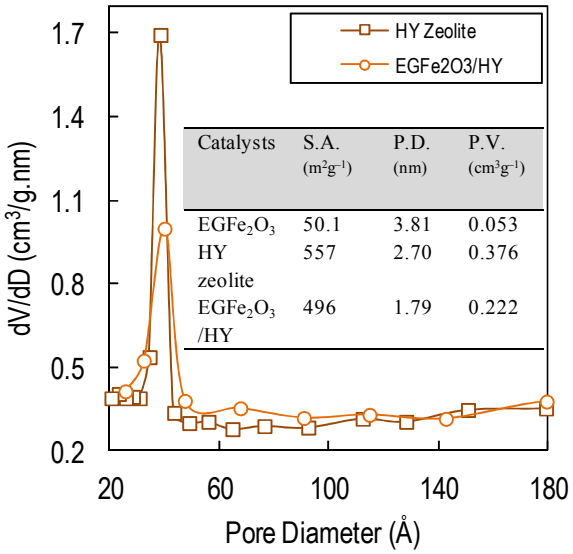

Catalysts	S.A. (m^2g^{-1})	P.D. (nm)	P.V. (cm^3g^{-1})
$EGFe_2O_3$	50.1	3.81	0.053
HY zeolite	557	2.70	0.376
$EGFe_2O_3$ /HY	496	1.79	0.222

Fig. 4. The pore size distribution curves of the photocatalysts, and the insert table shows the textural properties of the photocatalysts.

3.1.5 Chemical oxidation state determination

XPS analysis was performed to determine the chemical states of the surface metal in the catalyst. Fig. 5 shows the XPS spectra of Fe_{2p} and O_{1s} for $EGFe_2O_3$/HY catalyst. There are two deconvolution peaks were observed in the Fe_{2p} at 711.7 eV ($Fe_{2p3/2}$) and 724.9 eV ($Fe_{2p1/2}$) (Fig. 5a). Both of the binding energy is similar to the reported values of 710.5 and 724.1 eV for Fe_{2p} in α-Fe_2O_3 [31]. However, the observed values for the catalysts material were slightly shifted to higher binding energies compared to pure metal oxide, which suggests strong interaction between iron and HY [32,33]. These peaks indicate the type of Fe occurred in the sample. Peaks at 709.5 eV and 722.75 eV indicated pure Fe while peaks at 712.75 eV and 726.25 eV indicated the bonded Fe with HY.

Next, the spectra of O_{1s} were obtained to differentiate the bonded oxygen atoms in silica environments. The photoelectron spectra of O_{1s} shown in Fig. 5b displays two peaks that

correspond to Si–O–Fe and Si–O–Si with binding energies of 530.1 and 532.9 eV [35]. The 530.1 eV peak that exists might be due to the increase in the ionic state of the oxygen bond when some of Si-O-Si groups convert to Si-O-Fe. The same phenomenon was observed by Simon *et al.,* (2005) when iron doping yttrium aluminosilicate glasses [36]. The XPS spectrum of Fe_{2p} and O_{1s} indicated that the valence state of Fe and O are +3 and -2, respectively.

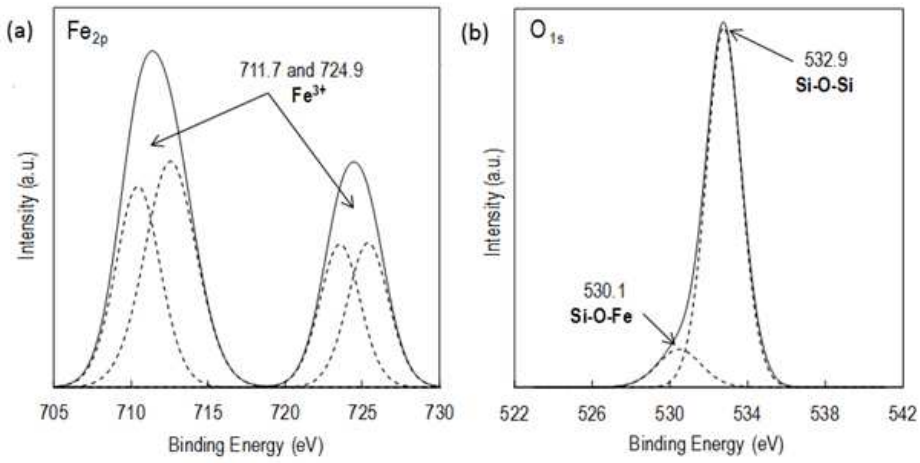

Fig. 5. XPS spectra of Fe_{2p} and O_{1s} for $EGFe_2O_3$/HY catalyst.

3.2. Photocatalytic testing for the decolorization of dyes

3.2.1. Effect of pH

The pH is most important parameters that influence the rate of photocatalytic activity [37]. Commonly, the multiple roles including electrostatic interactions between the catalyst surface, solvent molecules and substrate, and charged radicals formed during the reaction make an interpretation of the effect of pH is more difficult [11]. The effect of pH was studied in the range of 3–11 in presence of $EGFe_2O_3$/HY catalyst under sunlight conditions, and the results are

presented in Fig. 6. Each experiment was performed under dark conditions for 1 h to reach an adsorption–desorption equilibrium prior to photocatalytic reaction. The highest decolorization was obtained by MB with a complete decolorization at pH 11 (99.9%), followed by CR with 96.4% decolorization at pH 7, and MO with 91.3% decolorization at pH 5.

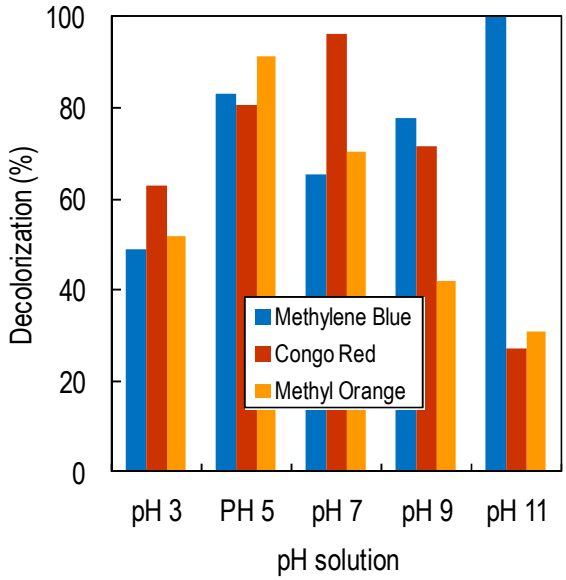

Fig. 6. Effect of pH on the decolorization of MB, CR, and MO dye. (C_o = 10 mg L^{-1}; W = 0.38 g L^{-1}; t = 2 h; 1 wt% $EGFe_2O_3$/HY; under sunlight irradiation)

At pH 11, the MB cations are easily attracted to the catalyst surface because of the low competition given by the abundance of hydroxyl anions in the solution. Direct exposure of this state to sunlight increased the formation of hydroxyl radicals and the photocatalytic reaction rate, which led to an increase in MB decolorization up to 100% after 2 h of contact time (Fig. 6). Lowering the pH to acidic conditions will cause competition between the MB cations and H^+ ions that inhibit the MB dye from approaching the catalyst surface, thus reduced the efficiency of the photoreaction to 83.2% and 48.9% of the MB decolorization at pH 5 and pH 3, respectively.

316 In contrast, a neutral pH appears to decrease in the photocatalytic activity (65.5%). This may be
317 due to diminutive hydroxyl formation in neutral condition; resultant less radicals being generates
318 through an electron−hole pair, which is the most crucial factor for initiation of the
319 photodecolorization activity. Therefore, the reaction did not perform well under neutral
320 condition. This occurrence was identical to our previous reported regarding to the
321 photodecolorization of MB using EGZrO_2/HY zeolite at optimum pH 11 [23].

322 In contrary, the CR shows the optimum pH value at 7 after 2 h when exposure to sunlight
323 irradiation (Fig. 6). This observation is quite similar to the reported study [38]. The reduction on
324 decolorization was occurred at lower pH, which gave 80.6% and 62.8% of CR decolorized at pH
325 5 and pH 3, respectively. The surface of the photocatalyst becomes more negatively charged at
326 higher pH value which could repel the CR anions, hence gave about 71.4% and 27.1% of CR
327 decolorization at pH 9 and pH 11, respectively.

328 The MO dye generally has two chemical structures dependent on the pH value of solution.
329 Quinoid structure is a main form at low pH value, while azo structure at high pH value. In Fig. 6,
330 it was observed that MO molecules were readily decolorized when the pH was 5. The efficiency
331 of decolorization was significantly effective in the appropriate acidic solution, which accounted
332 of 51.6% and 91.3% for pH 3 and pH 5, respectively. In alkaline solution, when pH was 11 and
333 9, the decolorization efficiency was only 30.7% and 42.0%, respectively. However, at pH 7, the
334 decolorization was found to be 70.4%. It is indicates that the photocatalytic activity of the
335 EGFe_2O_3/HY in acidic solutions is higher than the basic solutions. The suitability of MO to be
336 decolorized under alkaline conditions was also reported in literature [39]. Thus, it is confirms
337 that the primary factor affecting the substrate decolorization in the system is pH. Difference
338 types of dye could achieve difference rate of decolorization, at variance of pH environment.
339

340 *3.2.2. Effect of catalyst dosage*

The effect of catalyst dosage on the difference types of dye decolorization was studied in range from 0.08 to 0.68 g L^{-1}, and the results were shown in Fig. 7. Increase in the number of active sites towards higher catalyst dosage contributing to an increase in the number of photons and dye molecules absorbed, thus increase in decolorization [31]. It was observed that the most effective decolorization of dye use was achieved with a catalyst dosage of 0.38 g L^{-1}, and a further increase in catalyst dosage resulted in a decrease in decolorization. Higher turbidity of the suspension due to higher particle concentration leads to the reducing of light penetration and inhibits photodecolorization [40].

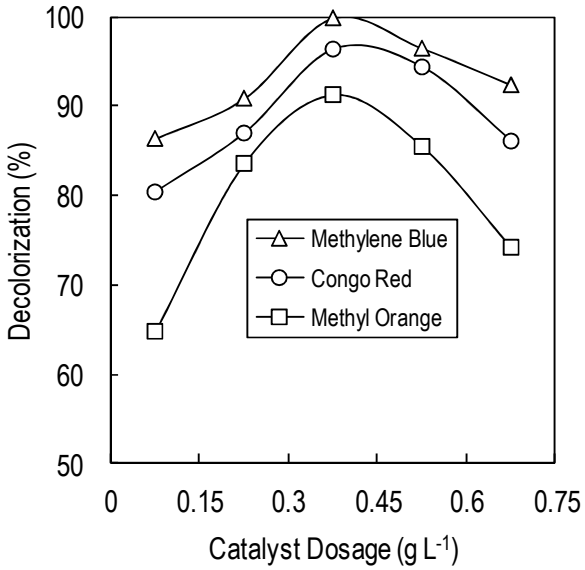

Fig. 7. Effect of catalyst dosage on the decolorization of MB, CR, and MO dye. (C_o = 10 mg L^{-1}; pH_{MB} = 11, pH_{CR} = 7, pH_{MO} = 5; t = 2 h; 1 wt% EGFe_2O_3/HY; under sunlight irradiation)

3.2.3. Photocatalytic performance of validation and confirmation

The photocatalytic performance of validation and confirmation of the prepared $EGFe_2O_3$/HY catalyst for the decolorization of MB, MO, and CR was examined, and the results are shown in Fig. 8. A controlled experiment was conducted under four different conditions including photolysis and the reaction in the presence of the bare HY, $EGFe_2O_3$, and $EGFe_2O_3$/HY catalysts. Each experiment was performed under both dark and sunlight conditions. The experiments under dark conditions removed less than 19% of the dyes after 2 h of contact time, which indicated the importance of sunlight in this study, as revealed by the optical properties study. Under photolysis, 3.1% of the MB, 1.2% of the CR and 0.6% of the MO was decolorized; this might due to the degradation of the substance after long exposure to sunlight. In addition, only 12.4% and 4.9% of the MB, 3.1% and 0.6% of the CR, and 8.3% and 2.1% of the MO was removed when using bare HY under dark and sunlight conditions, respectively. The porosity of the catalyst surface may play an important role in adsorption, as previously reported for liquid−gas adsorption systems used to treat wastewater [21]. The use of $EGFe_2O_3$ catalyst under sunlight resulted in 31.8%, 36.7%, and 28.4% decolorization of MB, CR, and MO which was approximately 2 − 8 times higher than the same reaction under dark conditions, respectively. However, the removal percentage was increased up to 99.9% for MB, 96.4% for CR, and 91.3% for MO when using 1 wt% $EGFe_2O_3$/HY. Good distribution with highly dispersed of the $EGFe_2O_3$ nanoparticles on the surface of the HY accompanied by synergistic effects might facilitate their surface contact with light, which led to higher efficiency of decolorization. This result reveals that $EGFe_2O_3$/HY is a potential photocatalyst semiconductor for dyes removal.

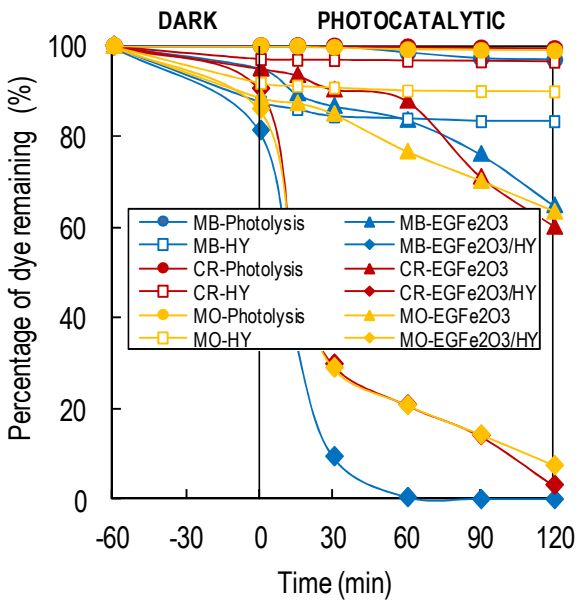

Fig. 8. Photocatalyst performance on the decolorization of MB, CR, and MO. (C_o = 10 mg L^{-1}; pH_{MB} = 11, pH_{CR} = 7, pH_{MO} = 5; W = 0.38 g L^{-1}; t = 2 h)

3.3. Kinetic analysis

The kinetics study of MB, MO, and CR photodecolorization were performed using a series of reactions by following the optimum conditions of every single dye, respectively, and were conducted under different initial concentrations of dye ranging from 10 to 100 mg L^{-1} (Table 1). The concentration of 10 mg L^{-1} for each dye gave the highest rate of decolorization after 2 h of irradiation. Lower efficiency of photodecolorization was observed at higher dye concentration due to the formation of several layers of adsorbed dye on the catalyst surface, and no direct contact of the catalyst with photogenerated holes or hydroxyl radicals that prevented the dye molecules from reaching the catalyst surface to adsorb light and photons [37].

Table 1. The parameters of photodecolorization at different initial concentration of MB, CR, and MO dye.

Initial concentration (mg L^{-1})	Reaction rate, k (min^{-1})			Initial reaction rate, r_o (mg L^{-1} min^{-1})			Decolorization (%)		
	Types of dye								
	MB[a]	CR[b]	MO[c]	MB[a]	CR[b]	MO[c]	MB[a]	CR[b]	MO[c]
10	0.0766	0.0256	0.0213	0.766	0.256	0.213	99.9	96.4	91.3
20	0.0326	0.0179	0.0098	0.652	0.358	0.196	90.0	89.8	70.8
30	0.0140	0.0147	0.0069	0.420	0.441	0.207	57.2	84.1	55.9
50	0.0086	0.0087	0.0051	0.430	0.435	0.255	41.0	63.5	43.6
70	0.0063	0.0053	0.0039	0.441	0.371	0.273	30.8	46.4	35.7
100	0.0052	0.0038	0.0027	0.520	0.380	0.270	25.9	38.3	25.5

[a] MB – Methylene Blue ; [b] CR – Congo Red ; [c] MO – Methyl Orange

In the previous study, it was confirms the photocatalytic decolorization rate was described by pseudo first−order kinetics, which is rationalized in terms of the Langmuir–Hinshelwood model [23]. This indicates that the reactions occurring at a solid–liquid interface. Integration of the simplest Eq. (5) for the rates of photodecolorization yields Eq. (6):

$$\ln C_t = -kt + \ln C_0 \quad (5)$$

$$\ln\left(\frac{C_0}{C_t}\right) = kt \quad (6)$$

where k is the pseudo first–order rate, C_o and C_t are the concentrations of dyes at initial and time t, respectively.

Theoretically, the straight line of a plot of $ln\ (C_o/C_t)$ as a function of time confirmed the reaction follows first–order kinetics (Fig. 9a). The slope of the line is the apparent first–order rate constant (k_{app}), and the values of k obtained from these experiments are listed in Table 1. It is well–recognized that the concentrations of dyes in the wastewater from textile industry effluents are always in the range of 0.01–0.05 g L^{-1} [13]. For that reason, the suitability of this system for low dye concentrations was in ordered to the higher value of first–order rate constant gave by a lower concentration of dye.

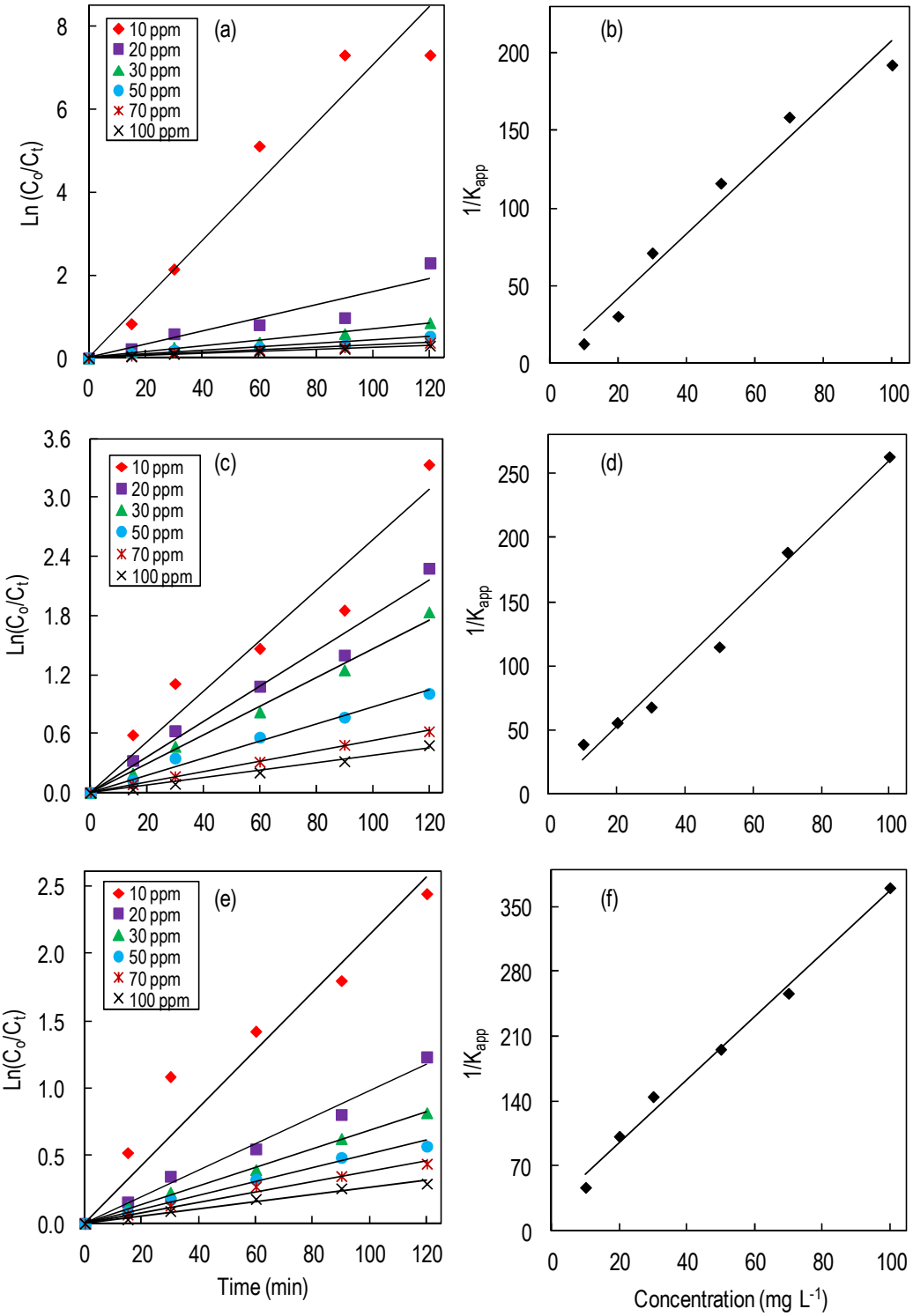

417

Fig. 9. Photodecolorization kinetics of (a) MB, (c) CR, and (e) MO using 1 wt% $EGFe_2O_3$/HY at different dye concentrations, and the relationship between $1/k_{app}$ and initial concentration of (b) MB, (d) CR, and (f) MO dye.

The photocatalytic activity of dye decolorization could be an interface process which might follow the Langmuir–Hinshelwood model (Eqs. 7 and 8):

$$r_0 = -\frac{dC}{dt} = \frac{K_R K_{LH} C_0}{1 + K_{LH} C_0} = k_{app} C_0 \quad (7)$$

$$\frac{1}{k_{app}} = \frac{1}{K_R K_{LH}} + \frac{C_0}{K_R} \quad (8)$$

where K_R is the reaction rate constant and K_{LH} is the Langmuir–Hinshelwood adsorption equilibrium constant.

Fig. 9b demonstrated a linear plot of $1/k_{app}$ as a function of C_o, verified that the photodecolorization of dye by $EGFe_2O_3$/HY is consistent with the Langmuir–Hinshelwood model. The reaction rate constant and the adsorption equilibrium constant were calculated to be K_R = 0.48 mg $L^{-1}min^{-1}$, K_{LH} = 3.83 L mg^{-1} for MB; K_R = 0.39 mg $L^{-1}min^{-1}$, K_{LH} = 1.78 L mg^{-1} for CR; and K_R = 0.29 mg $L^{-1}min^{-1}$, K_{LH} = 0.13 L mg^{-1} for MO. The value of $K_{LH} > K_R$ was obtained for both MB and CR dye suggested that the reaction would occur in the bulk of the solution as well as at the surface of the catalyst, and the number of adsorption sites may also not be abundant enough to initiate the reaction [23]. In contrast, the MO dye shows the value of $K_R > K_{LH}$ suggested that the dye adsorption was the controlling step of the process [12].

3.4. Leaching and reusability study

The samples were kept in the dark for 1 h, and then irradiated under sunlight for 2 h before being subjected to ICP–MS to study the effect of iron leaching into the solution. The results showed that no Fe ions were detected, indicating the photocatalytic occurrence is mainly due to the Fe that exists on the catalyst surface. Further, the reusability of $EGFe_2O_3$/HY catalyst was evaluated towards the photocatalytic activity of MB, CR, and MO decolorization (Fig. 10). The initial concentration of the dye used was maintained constant at 10 mg L^{-1}, and follows the previous optimum conditions, respectively. The catalyst was regenerated after filtration and calcination at 523 K for 3 h at every cycle. A slight decrease less than 13% was observed for every single dye with no obvious catalyst deactivation, indicating the reaction could be maintained after five cycling runs [11,12,23,24,41-43].

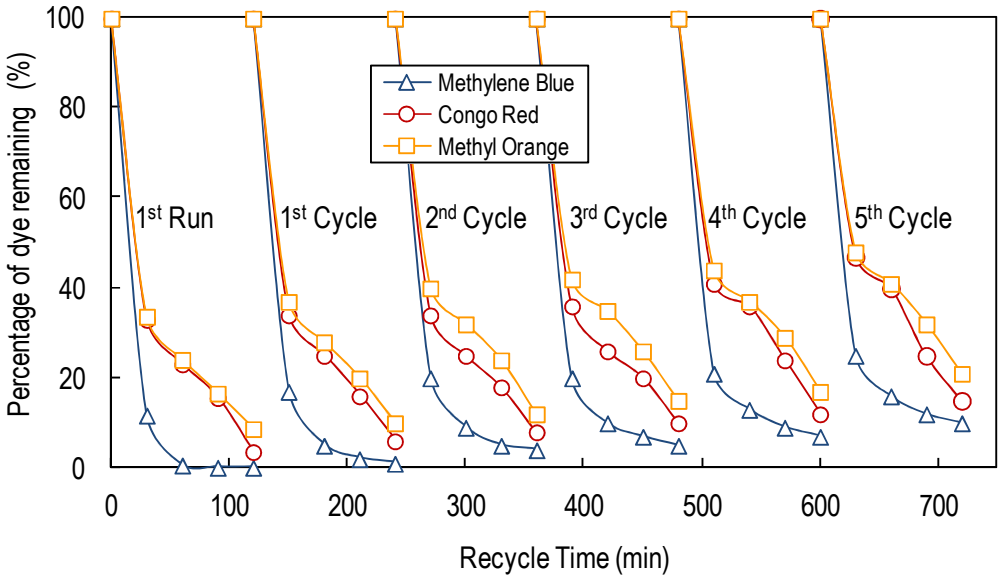

Fig. 10. Reusability and regeneration of 1 wt% $EGFe_2O_3$/HY on the photocatalytic decolorization of MB, CR, and MO dye. (C_o = 10 mg L^{-1}; pH_{MB} = 11, pH_{CR} = 7, pH_{MO} = 5; W = 0.38 g L^{-1}; t = 2 h, under sunlight irradiation)

3.5. Investigation on the simulated dyes and biodegradability

Since that the wastewater contains a lot of color and has a toxic odour, the removal of color from wastewater is more significant than the removal of other organic colorless chemicals [44]. Therefore, the change in the color of the simulated dyes over $EGFe_2O_3$/HY catalyst was examined under sunlight irradiation for a different time intervals, and shown in Fig. 11a. The color was disappeared steadily with increased in irradiation time, and the decolorization efficiency is inversely related to the dye concentration. A new dark green color was observed from a mixture of MB, CR, and MO dye; is believed to generate a new peak that appears at 291 nm and 244 nm in the system. However, these peaks were also diminished with the increased in time of irradiation.

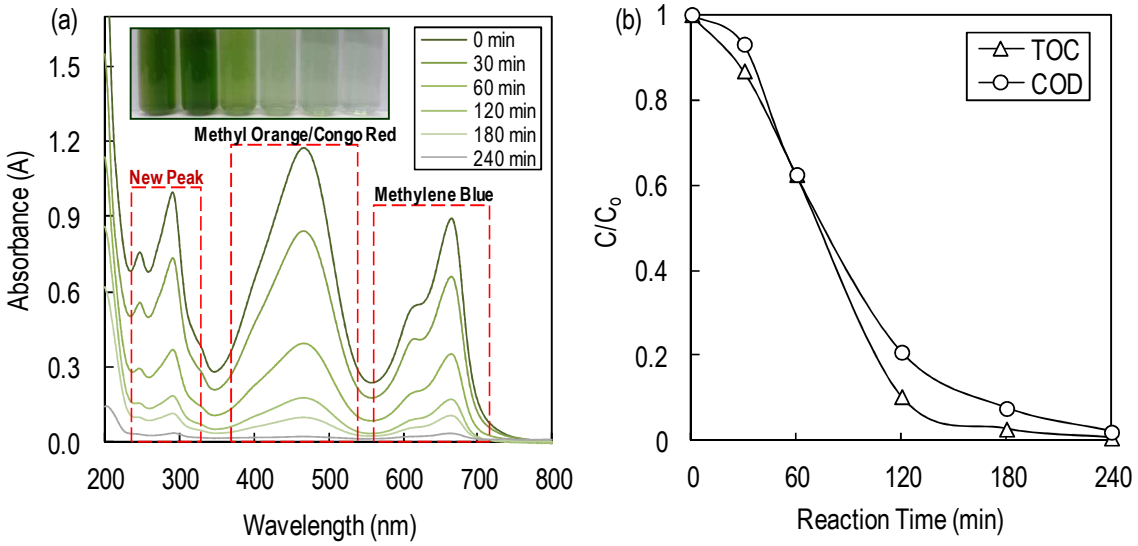

Fig. 11. (a) Photography image represents change in color of simulated dyes and UV spectra of the decolorization progress, and (b) the graph of COD and TOC reduction levels. (C_o = 10 mg L^{-1}; pH = 7; W = 0.38 g L^{-1}; t = 4 h; 1 wt% $EGFe_2O_3$/HY; under sunlight irradiation)

In general, the color degradation is closely related to TOC data [13,45]. Fig. 10b shows TOC and COD results for degradation of simulated dyes for different intervals of time. The TOC and COD results exhibit that the concentration of dyes decreases significantly with increasing time of sunlight irradiation. The catalyst exhibits high photocatalytic activity not only in the decolorization but also in the mineralization of colorless organic pollutants.

3.6. Proposed reaction mechanism of photocatalytic activity

In this study, both of the $EGFe_2O_3$ and HY were verified plays an important role in enhancing the photodecolorization of organic dyes. Hence, a proposed reaction mechanism of the photocatalytic activity of the decolorization of dyes was illustrated in Fig. 12. In relation to the presence of Fe^{3+} ions, the photocatalytic decolorization of MB, MO, and CR dye are proposed as follows; irradiated $EGFe_2O_3$/HY under sunlight generates electron–hole pair, and (Fe^{3+}) ions of $EGFe_2O_3$ are also crucial species that would take parts in the subsequent reaction [19].

$$EGFe_2O_3 + h\nu \rightarrow EGFe_2O_3\left(h^+_{VB} + e^-_{CB}\right) \quad (9)$$

$$EGFe_2O_3\left(Fe^{3+}\right) \rightarrow EGFe_2O_{3_{vacancy}} + Fe^{3+} \quad (10)$$

The electron in the conduction band (e^-_{CB}) is highly potential and negatively enough to reduce Fe^{3+} to Fe^{2+}, but then re–oxidizes to Fe^{3+} to ensure the formation of $O_2^{\cdot}$ radicals. Subsequent reaction of the Fe^{2+} with the formed partial $O_2^{\cdot}$ radicals resulted in formation of H_2O_2.

$$EGFe_2O_3\left(Fe^{3+}\right)+e^{-}_{CB}\rightarrow EGFe_2O_3\left(Fe^{2+}\right) \quad (11)$$

$$EGFe_2O_3\left(Fe^{2+}\right)+O_2\rightarrow EGFe_2O_3\left(Fe^{3+}\right)+O_2^{\cdot} \quad (12)$$

$$H^{+}+O_2^{\cdot}\rightarrow HO_2^{\cdot}\left(partial\ O_2^{\cdot}\right) \quad (13)$$

$$EGFe_2O_3\left(Fe^{2+}\right)+HO_2^{\cdot}\left(partial\ O_2^{\cdot}\right)+H^{+}\rightarrow EGFe_2O_3\left(Fe^{3+}\right)+H_2O_2 \quad (14)$$

On the other hand, the valence band hole (h^{+}_{VB}) potential is positively enough to generated hydroxyl radicals on the surface. The high oxidative potential of holes can lead to direct (Eq. 23) and indirect (Eqs. 16 and 22) oxidation of dye [11].

$$OH^{-}_{ads}+h^{+}_{VB}\rightarrow\cdot OH_{ads} \quad \text{(in basic medium)} \quad (15)$$

$$H_2O_{ads}+h^{+}_{VB}\rightarrow\cdot OH_{ads}+H^{+} \quad (16)$$

Electron in the conduction band (e^{-}_{CB}) on the catalyst surface also reduced molecular oxygen to superoxide anion,

$$O_{2(ads)}+e^{-}_{CB}\rightarrow\cdot O^{-}_{2ads} \quad (17)$$

The radical O_2^{-} species was responsible for the production of hydroxyl and hydrogen peroxides radicals:

$$\cdot O^{-}_{2(ads)} + H^{+} \rightarrow HO^{\cdot}_{2(ads)} \quad \text{(in acidic medium)} \tag{18}$$

$$2OH^{\cdot}_{ads} \rightarrow O_2 + H_2O_2 \tag{19}$$

$$H_2O_2 + \cdot O^{-}_{2(ads)} \rightarrow O_2 + HO^{\cdot} + HO^{-} \tag{20}$$

$$\cdot O^{-}_{2(ads)} + HO^{\cdot}_{2(ads)} + H^{+} \rightarrow H_2O_2 + O_2 \tag{21}$$

Therefore, it could be concluded that the ions (Fe^{3+}) of the $EGFe_2O_3$ are active catalytic species which leads to the formation of the three highly reactive radicals; hydroxyl ($HO^{\cdot}$), hydrogen peroxides ($HO_2^{\cdot}$) and superoxide ($^{\cdot}O_2^{-}$) for the MB, CR, and MO oxidation. The high oxidation potential of the holes (h^{+}_{VB}) in the photocatalyst also permits the direct oxidation of MB, CR, and MO to reactive intermediates.

$$Dye + OH^{\cdot} \rightarrow decolorization\ of\ dye \tag{22}$$

$$Dye + h^{+}_{VB} \rightarrow oxidation\ of\ dye \tag{23}$$

$$Dye + e^{-}_{CB} \rightarrow reduction\ of\ dye \tag{24}$$

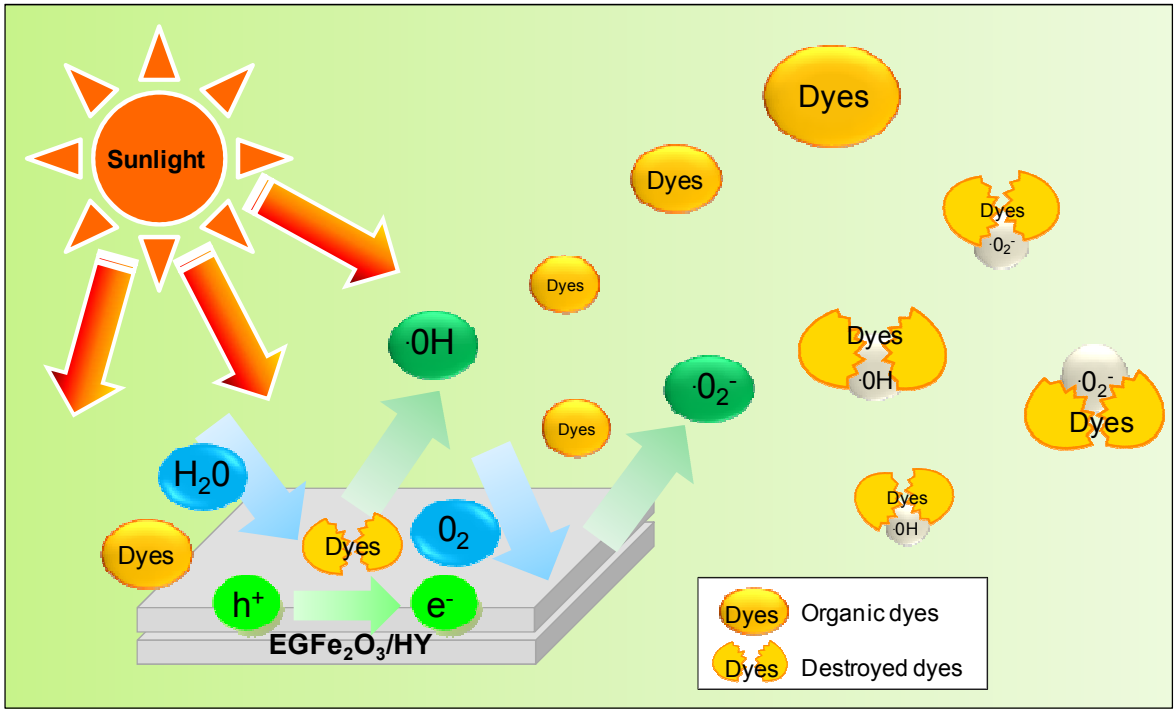

Fig. 12. Schematic diagram of a proposed reaction mechanism for the photodecolorization of dyes.

4. Conclusions

In this study, we have introduced a facile electrosynthesis method of $EGFe_2O_3$/HY with highly dispersed < 30 nm in size $EGFe_2O_3$ nanoparticles onto HY surface for superior decolorization of methylene blue (MB), congo red (CR), and methyl orange (MO) dye. The MB dye shows the highest decolorization which accounted of 99.9%, followed by CR (96.4%), and MO (91.3%) under particular optimum conditions. The photocatalytic performance of validation and confirmation was carried out to reveals that $EGFe_2O_3$/HY is a potential photocatalyst semiconductor for dyes removal under sunlight irradiation. The photoreaction follows pseudo first–order kinetics, and the rate constants was determined using the Langmuir–Hinshelwood model that gave K_R = 0.48 mg $L^{-1}h^{-1}$ and K_{LH} = 3.83 L mg^{-1} for MB; K_R = 0.39 mg $L^{-1}h^{-1}$ and

559 K_{LH} = 1.78 L mg^{-1} for CR; and K_R = 0.29 mg $L^{-1}h^{-1}$ and K_{LH} = 0.13 L mg^{-1} for MO. There is no
560 leaching of $EGFe_2O_3$ ions was found during the photoreaction, hence for this reason, the
561 photocatalyst could be maintained with a slight decrease of decolorization (<13%) after five
562 cycling runs. The prepared $EGFe_2O_3$/HY photocatalyst was also demonstrated a good
563 performance for decolorization of the simulated dyes, a mixture of MB, CR, and MO dyes
564 solution. Nearly complete mineralization was observed for the simulated dyes when measured by
565 COD and TOC removal. An appropriate proposed photocatalytic mechanism was also discussed
566 in details. This system is believe to exhibits a great potential for improving the quality of
567 wastewater discharged from the textile industry due to the simple process of preparing the
568 catalyst with the low amount of metal loaded required.
569
570 **Acknowledgements**
571
572 The authors are grateful for the financial support by the Research University Grant from
573 Universiti Teknologi Malaysia (Grant No. 01H59), the awards of UTM-RMC Postdoctoral
574 Fellowship and UTM Zamalah Scholarship (Norzahir Sapawe), and special thanks to Associate
575 Professor Dr Aishah Abdul Jalil and Professor Dr Sugeng Triwahyono for their supports, help
576 and guidance throughout the research.
577
578 **References**
579
580 [1] N.M. Mahmoodi, *J. Taiwan Inst. Chem. Eng.*, 2013, **44**, 322–330.
581 [2] S. Dawood and T.K. Sen, *Water Research*, 2012, **46**, 1933–1946.
582 [3] C.D.S. Rodrigues, L.M. Madeira, R.A.R. Boaventura, *J. Hazard. Mater.*, 2009, **172**, 1551–
583 1559.

[4] R.A. Damodar, S.J. You and S.H. Ou, *Sep. Purif. Technol*., 2010, **78**, 64–71.

[5] N. Sapawe, A.A. Jalil, S. Triwahyono, M.I.A. Shah, R. Jusoh, N.F.M. Salleh, B.H. Hameed and A.H. Karim, *Chem. Eng. J*., 2013, **229**, 388–398.

[6] J. Miao, Z. Jia, H.B. Lu, D. Habibi, L.C. Zhang, *J. Taiwan Inst. Chem. Eng.*, 2014, **45**, 1636–1641.

[7] N. Sapawe, A.A. Jalil, S. Triwahyono, *Malaysian J. Fundamental Appl. Sci.*, 2013, **9**, 67–73.

[8] A.A. Jalil, S. Triwahyono, M.R. Yaakob, Z.Z.A. Azmi, N. Sapawe, N.H.N. Kamarudin, H.D. Setiabudi, N.F. Jaafar, S.M. Sidik, S.H. Adam and B.H. Hameed, *Bioresource Technol*., 2012, **120**, 218–224.

[9] M. Aleksic, H. Kusic, N. Koprivanac, D. Leszczynska and A.L. Bozic, *Desalination*, 2010, **257**, 22–29.

[10] N. Sapawe, N.F. Jaafar, N.H.H. Hairom, M.A.H. Satar, M.N. Ariffin, S. Triwahyono, A.A. Jalil, *J. Fundamental Sci.*, 2011, **7**, 19–23.

[11] A.A. Jalil, M.A.H. Satar, S. Triwahyono, H.D. Setiabudi, N.H.N. Kamarudin, N.F. Jaafar, N. Sapawe and R. Ahamad, *J. Electroanal. Chem*., 2013, **701**, 50–58.

[12] N.F. Jaafar, A.A. Jalil, S. Triwahyono, M.N.M. Muhid, N. Sapawe, M.A.H. Satar and H. Asaari, *Chem. Eng. J*., 2012, **191**, 112–122.

[13] J. Grzechulska and A.W. Morawski, *Appl. Catal. B: Environ*., 2002, **36**, 45–51.

[14] M.C. Roco, *Curr. Opin. Biotechnol*., 2003, **14**, 337–346.

[15] S.H. Huang, M.H. Liao and D.H. Chen, *Biotechnol. Prog*., 2003, **19**, 1095–1100.

[16] A.K. Gupta and M. Gupta, *Biomater*., 2005, **26**, 3995–4021.

[17] Z.M. El–Bahy, M.M. Mohamed, F.I. Zidan and M.S. Thabet, *J. Hazard. Mater*., 2008, **153**, 364–371.

[18] W. Zhang, K. Wang, Y. Yu and H. He, *Chem. Eng. J*., 2010, **163**, 62–67.

[19] A. Nezamzadeh–Ejhieh and S. Hushmandrad, *Appl. Catal. A: Gen*., 2010, **388**, 149–159.

609 [20] D.R. Liu, Y.S. Jiang, G.M. Gao, *Chemosphere*, 2011, **83**, 1546–1552.

610 [21] H. Chen, A. Matsumoto, N. Nishimiya and K. Tsutsumi, *Colloids Surf. A: Physicochem.*

611 *Eng. Asp*., 1999, **157**, 295–305.

612 [22] N. Sapawe, A.A. Jalil, S. Triwahyono, R.A.R.N. Sah, N.W.C. Jusoh, N.H.H. Hairom, J.

613 Efendi, *Appl. Catal. A: Gen.*, 2013, **456**, 144–158.

614 [23] N. Sapawe, A.A. Jalil, S. Triwahyono, S.H. Adam, N.F. Jaafar, M.A.H. Satar, *Appl. Catal.*

615 *B: Environ.*, 2012, **125**, 311–323.

616 [24] N. Sapawe, A.A. Jalil and S. Triwahyono, *Chem. Eng. J*., 2013, **225**, 254–265.

617 [25] A.A. Jalil, S. Triwahyono, N. Sapawe, I.H. Ahmed, M.A.A. Aziz, Desalin. *Water Treat.*,

618 2014, 1–15.

619 [26] W.J. Liu, F.X. Zeng, H. Jiang, X.S. Zhang and W.W. Li, *Chem. Eng. J*., 2012, **180**, 9–12.

620 [27] W. Zhang, K. Wang, Y. Yu, H. He, *Chem. Eng. J.*, 2010, **163**, 62–67.

621 [28] C.J. Lucio–Ortiz, J. Rivera de la Rosa, A. Hernandez–Ramirez, E.M. Lopez–Cuellar, G.

622 Beltran–Perez, R.D.C. Miranda Guardiola and C.D. Pedroza–Solis, *Colloids Surf. A:*

623 *Physicochem. Eng. Asp*., 2010, **371**, 81–90.

624 [29] H. Jia, H. Xu, Y. Hu, Y. Tang and L. Zhang, *Electrochem. Commun*., 2007, **9**, 354–360.

625 [30] J. Portier, H.S. Hilal, I. Saadeddin, S.J. Hwang, M.A. Subramanian and G. Campet, *Prog.*

626 *Solid State Chem*., 2004, **32**, 207–217.

627 [31] D.P. Das, N. Baliarsingh and K.M. Parida, *J. Mol. Catal. A: Chem*., 2007, **261**, 254–261.

628 [32] K. Hirokawa and M. Oku, *Talanta*, 1979, **26**, 855–859.

629 [33] R.B. Borade, A. Adnot and S. Kaliaguine, *Zeolites*, 1991, **17**, 710–719.

630 [34] M. Shimokawabe, T. Chaki, S. Ozawa and M. Arai, *React. Kinet. Catal. L.*, 2005, **86**, 363–

631 370.

632 [35] Y.H. Kim, D.K. Lee, H.G. Cha, C.W. Kim, Y.C. Kang and Y.S. Kang, 2006, *J. Phys. Chem.*

633 *B*, 2006, **110**, 24923–24928.

[36] V. Simon, D. Eniu, A. Taka'cs, K. Magyari, M. Neumann and S. Simon, *J. Non-Cryst. Solids*, 2005, **351**, 2365–2372.

[37] H. Lachheb, E. Puzenat, A. Houas, M. Ksibi, E. Elaloui, C. Guillard and J.M. Herrmann, *Appl. Catal. B: Environ*., 2002, **39**, 75–90.

[38] G. Annadurai, T. Sivakumar and S.R. Babu, *Bioprocess Eng*., 2000, **23**, 167–173.

[39] H. Ma, B. Wang and X. Luo, *J. Hazard. Mater*., 2007, **149**, 492–498.

[40] E. Bizani, K. Fytianos, I. Poulios and V. Tsiridis, *J. Hazard. Mater*., 2006, **136**, 85–94.

[41] N.W.C. Jusoh, A.A. Jalil, S. Triwahyono, H.D. Setiabudi, N. Sapawe, M.A. H. Satar, A.H, Karim, N.H.N. Kamarudin, R. Jusoh, N.F. Jaafar, N. Salamun and J. Efendi, *Appl. Catal. A: Gen*., 2013, **468**, 276–287.

[42] R. Jusoh, A.A. Jalil, S. Triwahyono, Ani Idris, S. Haron, N. Sapawe, N.F. Jaafar and N.W.C. Jusoh, *Appl. Catal. A: Gen*., 2014, **469**, 33–44.

[43] N. Sapawe, *New J. Chem.*, 2015, **39**, 4525–4533.

[44] G. Chen, L. Lei and P.L. Yue, *Ind. Eng. Chem. Res*., 1999, **38**, 1837–1843.

[45] A. Akyol, H.C. Yatmaz and M. Bayramoglu, *Appl. Catal. B: Environ*., 2004, **54**, 19–24.